THE AMERICAN SOCIETY OF MECHANICAL ENGINEERS
Three Park Avenue, New York, N.Y. 10016-5990

99-GT-246

A STUDY OF THE FLOW FIELD IN A MODEL ROTOR-STATOR DISK CAVITY

R.P.Roy, S.Devasenathipathy, G.Xu, and Y.Zhao
Arizona State University
Department of Mechanical and Aerospace Engineering
Tempe, Arizona

ABSTRACT

Experimental and computational studies of the turbulent flow field in a model gas turbine disk cavity have been carried out. The experiments were performed in a rig which features a rotor disk-stator disk configuration with stator vanes, rotor blades, and rim discouragers with axial overlap. Particle Image Velocimetry was used to map the flow field in the cavity at three positions along the axial gap between the disks for various mainstream and secondary air flow rates, and rotor speeds. Static pressure distribution in the cavity at the stator disk and the circumferential distribution of the same at the mainstream passage outer shroud were measured.

A recirculation region developed radially inboard in the disk cavity where a strong radial outflow was found close to the rotor disk and a weak radial inflow near the stator disk. This is the source region where the rotation of the core fluid is minimal, its radial extent increasing with the secondary air flow rate. Radially outboard, in the core region, the flow was rotation-dominated except when the secondary air flow rate was high.

The peak-to-peak amplitude of the circumferential pressure asymmetry in the mainstream flow path increased as the square of the main air flow rate, attained its maximum value at the stator vane exit, and decreased rapidly downstream. For the experiments performed, no circumferential pressure asymmetry could be found in the disk cavity, even near its rim. The rotating fluid in the core region of the cavity gave rise to an adverse radial pressure gradient, its magnitude increasing as the secondary air flow rate decreased. This feature can facilitate ingress of mainstream gas into the cavity.

Concurrently with the experiments, the flow field was simulated numerically using the commercial CFD code FLUENT/UNS. The agreement between the measurements and the computed results is generally good.

NOMENCLATURE

b	outer radius of disk cavity - Fig. 2(a)
c_1	velocity of mainstream flow at vane exit
$c_{p,max}$	nondimensional peak-to-peak amplitude of the circumferential pressure asymmetry, $\Delta p_{max}/Q$
c_w	nondimensional mass flow rate of secondary air ($= \dot{m}/\mu b$)
$c_{w,fd}$	nondimensional free disk pumping flow rate ($= \dot{m}_{fd}/\mu b$)
G	axial gap ratio ($= s/b$)
G_c	discourager radial clearance ratio ($= z_r/b$)
$\dot{m}$	mass flow rate of secondary air
$\dot{m}_{fd}$	free disk pumping mass flow rate
p	static pressure
p_{atm}	ambient pressure
Q	mainstream flow dynamic head at vane exit
r	radial coordinate
Re_m	mainstream flow Reynolds number ($= \rho V_m b/\mu$)
Re_ϕ	disk rotational Reynolds number ($= \rho \Omega b^2/\mu$)
s	axial gap between rotor and stator disks
V_m	mainstream flow axial velocity
V_r	radial velocity
$V_{r,c}$	radial velocity in the core
V_ϕ	tangential velocity
$V_{\phi,c}$	tangential velocity in the core
Δp_{max}	peak-to-peak amplitude of circumferential pressure asymmetry
x	axial coordinate
z_a	discourager axial overlap - Fig. 2(a)
z_r	discourager radial clearance - Fig. 2(a)
Greek symbols	
λ_{turb}	turbulent flow parameter ($= c_w\, Re_\phi^{-0.8}$)
μ	dynamic viscosity
ρ	density

Presented at the International Gas Turbine & Aeroengine Congress & Exhibition
Indianapolis, Indiana — June 7–June 10, 1999

Ω	angular speed of rotor disk
β	core fluid rotation ratio ($=V_\phi/\Omega r$)
ϕ	azimuthal coordinate

INTRDDUCTIDN

The next-generation land based and aircraft gas turbines will have a significantly higher inlet temperature than the present-day gas turbines. This is so that the turbine efficiency can be higher. Disk rotation coupled with circumferentially nonuniform static pressure distribution in the mainstream gas path creates a fluid-mechanical condition that can lead to ingress of the hot mainstream gas into rotor-stator disk cavities. This is an issue of serious concern because the ingested hot gas will adversely affect the thermo-mechanical state of the rotor disks and hence, their durability.

To counter the ingress of hot gas into the cavities, two steps have usually been taken : (1) discouragers are installed at the rim of the rotor and stator disks and labyrinth seals radially inboard; and (2) secondary (buffer) air bled from the compressor discharge is injected into the cavities at the hub and/or radially outboard, the air also helping cool the disks. Since the bleeding of the compressor air diminishes the overall performance of the gas turbine, it is necessary to accomplish the cavity sealing and disk cooling functions with the minimum amount of secondary air without risking disk failure. This, of course, requires comprehensive knowledge of the flow and thermal fields in the cavities.

In an earlier paper, Roy et al. (1997), we reported measurement and computation of the distributions of convective heat transfer coefficient and cooling effectiveness on the rotor disk surface in a model rotor-stator disk cavity. In the present paper, we report measurement and computation of the flow field in the same cavity at isothermal condition. First however, a brief survey of some of the past works relevant to the present work is presented.

In a pioneering work that was primarily experimental, Daily and Nece (1960) studied the flow field due to the rotation of a smooth plane disk enclosed within a right circular chamber. The cavity flow was classified into four different regimes depending on the axial gap ratio (G) and the disk rotational Reynolds number (Re_ϕ). Later, Daily et al. (1964) carried out a study of enclosed rotating disks with radially outward throughflow superposed on the fluid motion induced by the disk. Information on the steady mean velocity distribution, pressure distribution, and unsteady periodicities in the cavity were presented.

Some of the theoretical studies of rotor-stator cavity flow have been based on the momentum integral technique of von Karman (1921) - for example, Chew and Snell (1988). A more detailed study of the turbulent velocity and thermal fields in the cavity requires solution of the Reynolds-averaged Navier-Stokes equations (RANS), the thermal energy equation, and the equations of an appropriate turbulence model. Such an approach was taken by Gosman et al. (1976), Chew (1985), Louis and Salhi (1989), Ko and Rohde (1992), Virr et al. (1993), Ho et al. (1996), and Hills et al. (1997), among others.

Experimental studies of shrouded rotor-stator and/or rotor-rotor systems include those by Phadke and Owen (1988), Bhavnani et al. (1992), Dadkhah et al. (1992), and Green and Turner (1994). Investigations combining experiments and computations were conducted by Chew et al. (1994), Bohn et al. (1995), and Chen et al. (1996), among others.

A fluid-mechanical feature that is recognized as one key to the ingress of mainstream gas into the disk cavity is the circumferential pressure asymmetry in the mainstream flow. To obtain a realistic representation of this feature requires inlet vanes. Since rotor blades may be expected to influence this pressure distribution in some fashion, blades should also be incorporated in the rotor-stator configuration. Furthermore, discouragers on the stator and rotor disks are important. Very few of the aforementioned studies included all or even most of these features.

The overall scope of our undertaking is to carry out experiments and numerical simulations to better understand the turbulent flow field and convective heat transfer in gas turbine rotor-stator disk cavities. The rotor-stator configuration in which the experiments are performed is simpler than in actual gas turbines but retains the important features of stator vanes, rotor blades, and rim discouragers. Mainstream and secondary air are provided at various flow rates to the rotor-stator section by separate blowers. For the numerical simulations, we have used the commercial CFD code FLUENT/UNS (1998). In this paper, we specifically report the fluid velocity field on the radial (r) - azimuthal (ϕ) plane at three axial positions in the disk cavity. Particle image velocimetry (PIV) was used for these measurements which were performed at three disk rotational Reynolds numbers (Re_ϕ), three secondary air flow rates (c_w), and two mainstream flow rates (Re_m). Static pressure distributions were measured at the stator disk and at the outer shroud. The measurements are compared with the predictions of the code FLUENT/UNS in either the rotationally symmetric (two-dimensional) mode or the three-dimensional mode with azimuthally periodic (following the vane pitch) boundary conditions.

EXPERIMENTAL APPARATUS AND MDDELING TODL

The rotor-stator rig

Figures 1(a) and (b) are photographs of the rig. The mainstream air is supplied by a centrifugal blower (Hauck) equipped with a variable-frequency motor drive which provides a flow rate of upto 1.42 m^3/s ($\cong$ 3000 cfm). The air flow rate is measured by a pitot tube rake equipped with five pitot tubes located in the blower suction duct. The rotor-stator section is located on the suction side of the blower so that the section remains optically accessible from the radial direction as well as the axial (inlet) direction.

The secondary air is supplied by another centrifugal blower (Hauck) also equipped with a variable-frequency motor drive which provides a maximum flow rate of 0.12 m^3/s ($\cong$ 250 cfm). The secondary air flow rate is measured by a turbine flowmeter (EG&G Flow Technology).

The 0.403 m (15.875 inch) diameter aluminum rotor disk is equipped with 52 partial height blades ($\approx$one-third of engine height), Fig. 2(a). The partial blade height allows the axial velocity of the mainstream air to approach the rotor disk rim speed. A variable-frequency motor drive can rotate the disk up to a speed of 5000 rpm. The plexiglass stator disk, of the same diameter as the rotor disk, is equipped with 59 partial height vanes. The vanes turn the mainstream air by 55 degrees, imparting a realistic swirl to the flow.

A schematic of the rotor-stator sectioo is shown in Fig. 2. The rim discourager arrangement with an axial overlap of 2 mm and a radial clearance of 2 mm should be noted. Secondary air is supplied at the hub through a 38.1 mm i.d. pipe.

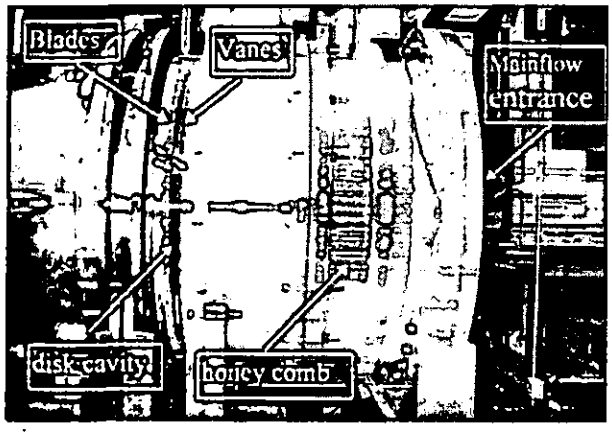

(a) inlet section

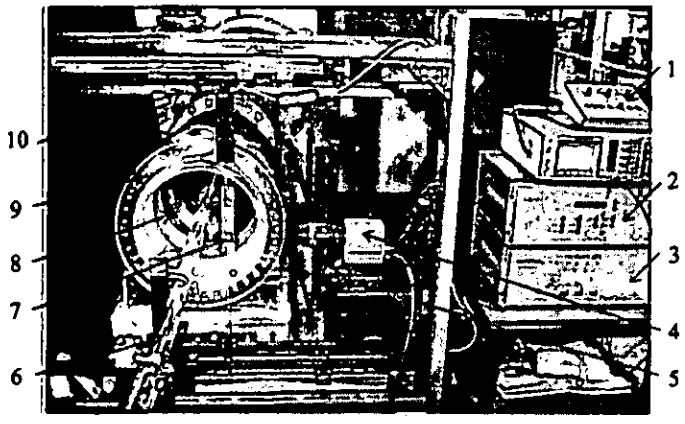

1. Remote control unit 2. Synchronizer 3. Mirror image shift
4. CCD camera 5. Traverse in vertical direction
6. Cooling tube 7. Rotating mirror 8. Stator disk
9 Main flow entrance 10. Traverse in horizontal direction

(b) the PIV set-up

Fig. 1 The rotor-stator disk cavity rig

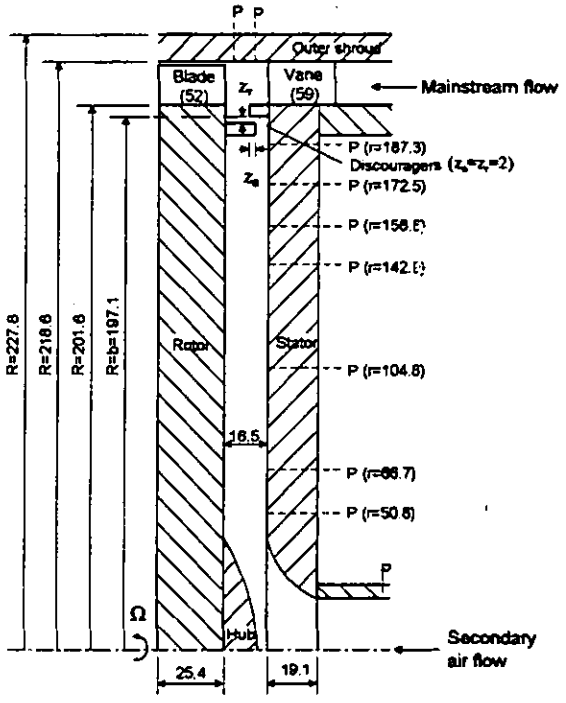

(a) The disk cavity

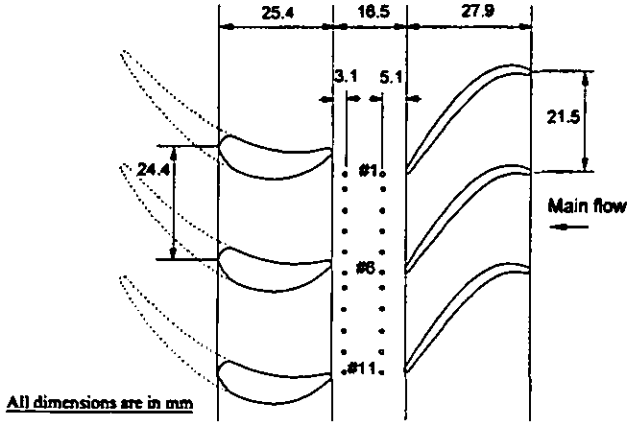

(b) Schematic of guide vanes and blades

Fig. 2 The model rotor-stator system

Measurement Techniques

(i) Particle Image Velocimetry (PIV)

In this imaging technique, the seeded (with particles or droplets) fluid is illuminated by a thin laser light sheet which is pulsed at a prescribed time interval. The seed image fields are recorded by a camera and then analyzed to obtain velocity information. Here, a dual Nd:YAG laser (Spectra-Physics PIV-200) was used which provides short duration (≈ 10 ns) pulses of 532 nm (green) light, the separation time between pulses being adjustable (100 ns to 100 ms). The light sheet generated by a combination of cylindrical and spherical lenses can be rendered a few micrometers to a few millimeters thick at the waist and several centimeters wide. A high resolution CCD camera (Kodak Megaplus 1.41, 1340×1037 pixels) captures an image pair on the same frame. Image shifting is introduced by a rotating mirror (TSI) located between the light sheet and camera to resolve directional ambiguity in the velocity field. The autocorrelation method is used for statistical evaluation of the seed particle (or droplet) velocity.

A Laskin's nozzle particle generator is used to produce olive oil droplets 1 to 2 μm in size that seed the secondary air supplied at the disk cavity hub.

Based on the camera pixel and array sizes and the magnification, the field of view of the current set-up on the r-ϕ plane of the disk cavity is approximately 67 mm × 53 mm. The thickness (along x) of the light sheet varies from approximately 100 μm at the waist to about 440 μm at the edge of the field of view. Mapping the region from the hub to the rim over an appropriate azimuthal sector required that the camera and the mirror be traversed in horizontal and vertical directions without changing their relative positions. This was achieved by mounting them in a common frame that can be traversed. A second traverse system allowed the light sheet optics to move vertically and horizontally. Note that optical access to the disk cavity is required from the periphery (for the light sheet) as well as through the stator disk (for the camera).

Three axial positions along the cavity axial gap were chosen for obtaining the r-ϕ plane velocity map – 3 mm from the rotor disk (x/s=0.182), 7 mm from the rotor disk (x/s=0.424), and 3 mm from the stator disk (x/s=0.818). At each position, the r-ϕ plane region of interest was subdivided into six sections (each 67 mm × 53 mm) and at each section, ten instantaneous velocity vector maps were obtained and then averaged to provide the mean map.

The viability of the PIV system along with the seed droplets was assessed by comparing its measurements at selected locations in the cavity with measurements by a three-hole pitot tube and by a one-component LDV system. The agreement was satisfactory.

(ii) Static pressure measurements

A differential pressure transducer (DPT) - digital manometer - Scanivalve system was used to measure static pressure distributions in the disk cavity at the stator disk and at the outer shroud. As shown in Fig. 2(a), pressure taps are located at seven radial locations on the stator disk. At the outermost radial location, r=187.3 mm (r/b = 0.95), eleven pressure taps have been provided circumferentially over an angle corresponding to two vane pitches. To examine the circumferential variation of static pressure in the mainstream flow, eleven pressure taps have also been provided circumferentially at the outer shroud, over two vane pitches, at two axial positions – one 5.1 mm downstream of vane trailing edge plane (x/s = 0.69) and the other 3.1 mm upstream of blade leading edge plane (x/s = 0.188).

The static gage pressure is measured by either a DPT (Validyne, 0 - ± 2 psid) or a digital manometer (Validyne, 0 - 0.07 psid) with one port open to the ambient for both transducers. The choice of transducer depends on the specific pressure being measured. The transducer pressure signals are routed to a data acquisition system (Analogic 6500).

Numerical Simulation Tool

The commercial CFD code FLUENT/UNS version 4.2 was used to calculate the flow field in the cavity and mainstream passage. The calculations were carried out in both the rotationally symmetric mode (all variables are ϕ-independent) dubbed the two-dimensional calculation in the remainder of this paper and the three-dimensional mode with azimuthally periodic (following the vane pitch) boundary conditions. Of the turbulence models provided in FLUENT, the renormalization group (RNG) k-ε model in conjunction with a two-layer (near-wall region, away-from-wall region) description of the flow domain was used in the two-dimensional calculations. The near-wall description was replaced by a wall function in the three-dimensional calculations.

Figure 5 (to be discussed later) shows the flow domain for the two-dimensional calculation. The vane was not included - instead, the swirl velocity imparted by the vane was added to the axial velocity of mainstream air and this provided as the velocity boundary condition at the vane trailing edge. In the three-dimensional simulation, the vane was included and the flow domain was circumferentially over one vane pitch with periodic boundary condition. The other flow boundary conditions were: the (exit) pressure at the blade leading edge plane and the secondary air velocity at the inlet pipe entrance.

RESULTS AND DISCUSSION

The results presented in this paper are drawa from seven experiments, Table 1. Selected computational results are also presented for these. Table 2 contains the uncertainties in the experiment parameters and the measured quantities for these experiments as estimated by an error propagation analysis. At higher disk rotational speed (and therefore higher fluid tangential velocities), the uncertainty in the fluid radial velocity may be higher than the value indicated in Table 2. This is because the radial velocity component, whose magnitude is typically much smaller than the tangential velocity magnitude especially toward the cavity rim, and the tangential velocity component are derived from the r- ϕ plane velocity vector measured by PIV.

Assuming turbulent boundary layer over the rotor disk, the free disk pumping flow rate, $\dot{m}_{fd}$, was calculated from the equation

$$\dot{m}_{fd}/(\mu b) = 0.219\,Re_{\phi}^{0.8} \qquad (1)$$

Table 1 Conditions for the seven experiments

Expt. No.	Re_ϕ	Re_m	c_w	$c_{w,fd}$
1	5.16×10^5	5.0×10^5	1504	8139
2	"	"	3008	"
3	"	"	7520	"
4	7.74×10^5	"	1504	11258
5	"	"	3008	"
6	9.55×10^5	"	1504	13319
7	"	6.2×10^5	"	"

Table 2 Estimated uncertainties

	Re_ϕ	Re_m	c_w	V_r	V_ϕ	p
Uncertainty	± 2 %	± 3 %	± 5 %	± 5 %	± 5 %	± 1 %

Velocity field

Figures 3(a) and 3(b) show, for experiment 5, the r-ϕ plane fluid mean velocity vector maps obtained by PIV at 3 mm from the rotor surface (x/s = 0.182) and 3 mm from the stator surface (x/s = 0.818), respectively. On the radially inboard half of the cavity, a strong radial outflow is indicated at the location near the rotor disk and a weaker radial inflow at the location near the stator disk. Radially outboard, the flow is dominated by the tangential velocity component at both axial positions. In Figs. 4(a) and (b), the fluid tangential and radial velocity components derived from the measured velocity vectors are plotted. The tangential velocity profiles at the three axial locations (all for the core fluid) are quite close to each other, increasing slightly in magnitude away from the rotor disk.

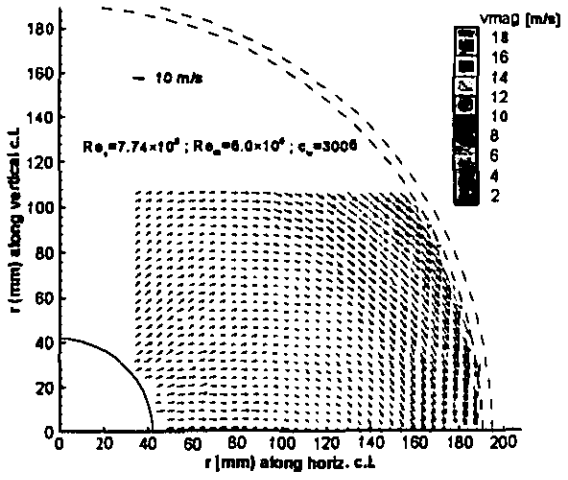

(a) 3 mm from the rotor disk surface

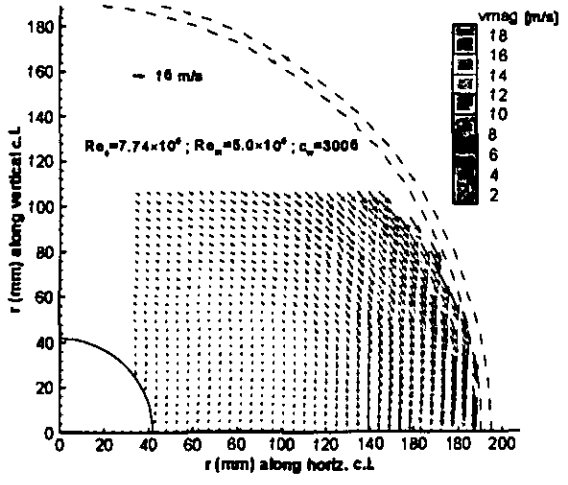

(b) 3 mm from the stator disk surface

Fig. 3 r-ϕ plane map of the fluid mean velocity in the cavity

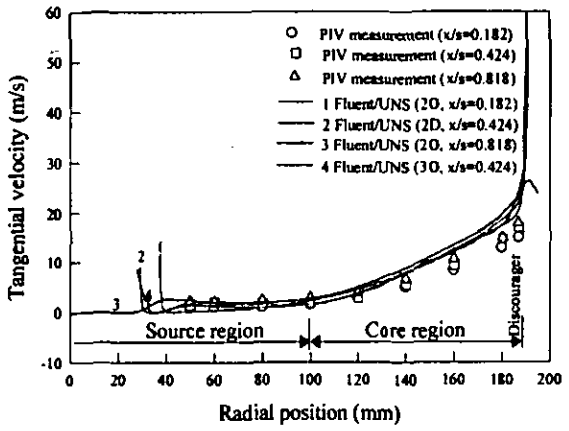

(a) Tangential velocity

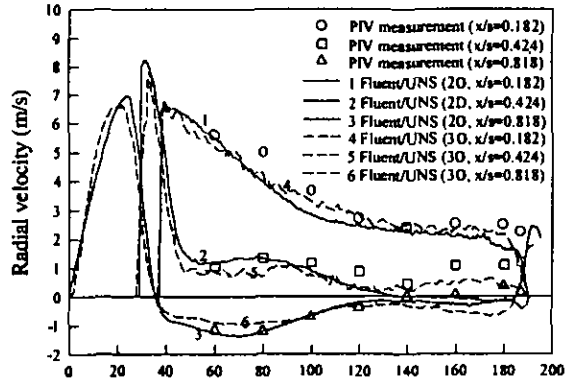

(b) Radial velocity

Fig. 4 Radial distribution of fluid tangential and radial velocities at $Re_\phi=7.74\times10^5$, $c_w=3008$ and $Re_m=5.0\times10^5$

The solid curves in these figures are results of FLUENT calculations. These results generally agree well with the measurements although the measured magnitudes are slightly lower than the calculated ones in the radially outboard half of the cavity. The fluid radial velocity in the radially outboard half of the cavity is much larger at the axial location near the rotor (x/s= 0.182) than at the two locations farther (x/s = 0.424 and 0.818). The tangential velocity remains very small and essentially invariant to r ≈ 100 mm and then increases with radius. The very low tangential velocity region is due to the superposed secondary air and is referred to as the "source region" in Fig. 4(a). The region radially outboard has been dubbed the "core region" in Fig. 4(b).

The radial velocity distributions of Fig. 4(b) may be understood better when studied in conjunctinn with the r-z plane streamlines obtained from the two-dimensional calculation, Fig. 5. In the source region, the outward radial velocity at 7 mm from the rotor (x/s= 0.424) and the inward radial velocity at 3 mm from the stator (x/s= 0.818) are due to a recirculation region. The large outward radial velocity near the rotor (x/s=0.182) is a compendium of the rotation-induced component and the component due to secondary air flow.

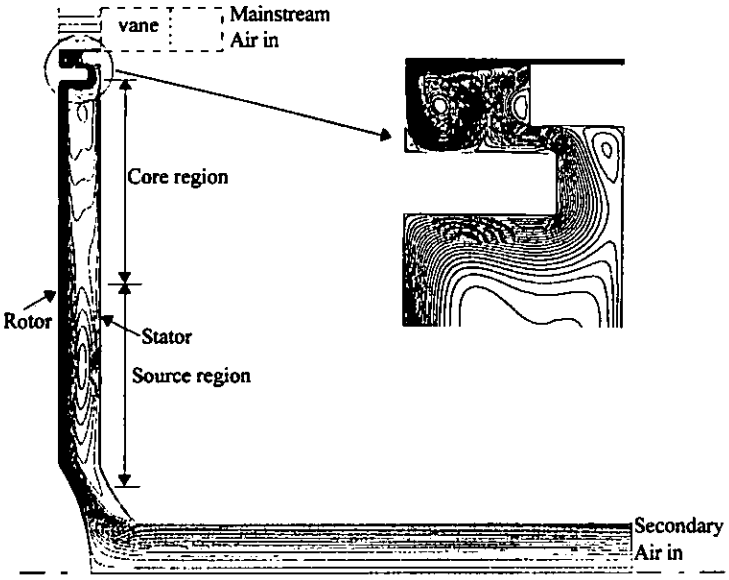

Fig. 5 Computed streamlines for Re_ϕ=7.74x10^5, c_w=3008, and Re_m=5.0x10^5

In the core region at larger radii (r > 150 mm), the tangential velocity of the fluid is considerably larger than the radial velocity. As has already been mentioned, a relatively large uncertainty is introduced in the measured radial velocity here.

The effect of secondary air flow rate, c_w, on the fluid tangential velocity near the mid-axial gap (x= 0.424) is shown in Figs. 6(a) and (b). Both experimental data and FLUENT results are shown. That the core rotation is almost completely suppressed in the case of Re_ϕ= 5.16x10^5 and c_w = 7520 can be seen, the secondary flow rate in this case being approximately 92 percent of the free disk pumping flow rate. The effect of c_w on the radial extent of the source region can also be observed, it increasing as c_w increases.

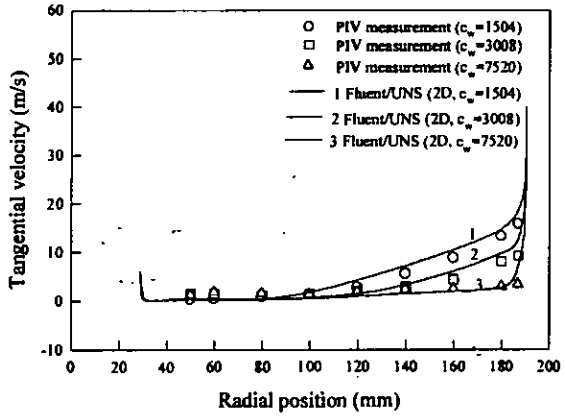

(a) Re_ϕ=5.16×10^5

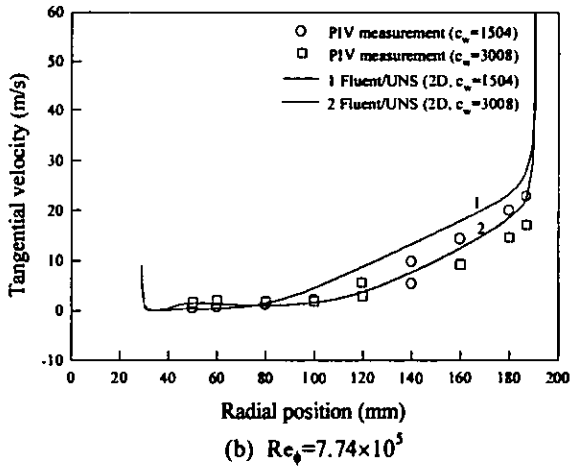

(b) Re_ϕ=7.74×10^5

Fig. 6 Effect of c_w on the fluid tangential velocity near the cavity mid-axial gap (x/s=0.424) for Re_m=5.0×10^5

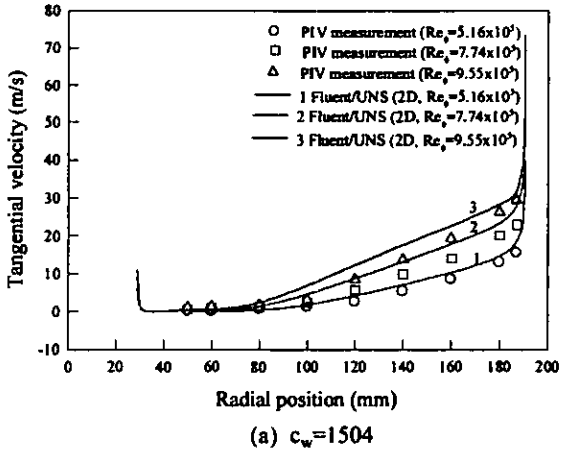

(a) c_w=1504

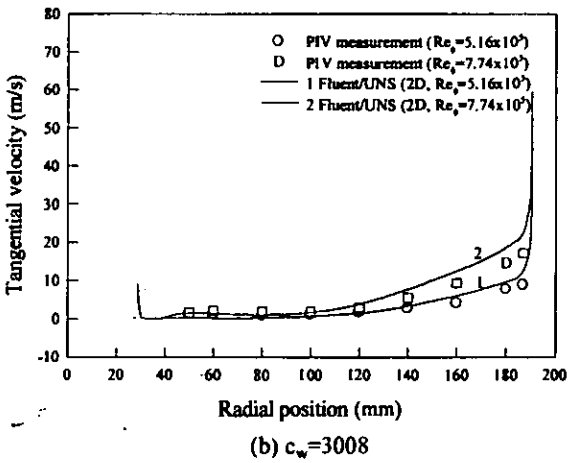

(b) c_w=3008

Fig. 7 Effect of Re_ϕ on the fluid tangential velocity near the cavity mid-axial gap (x/s=0.424) for Re_m=5.0×10^5

Figures 7(a) and (b) show the effect of rotational Reynolds number on the fluid mean tangential velocity near the cavity mid-axial gap (x/s = 0.424) for experiments 1, 2, and 3 through 6. At any particular secondary air flow rate, a higher rotor disk speed gives rise to a larger fluid tangential velocity in the core fluid. The radial extent of the source region is seen to decrease slightly with increasing Re_ϕ.

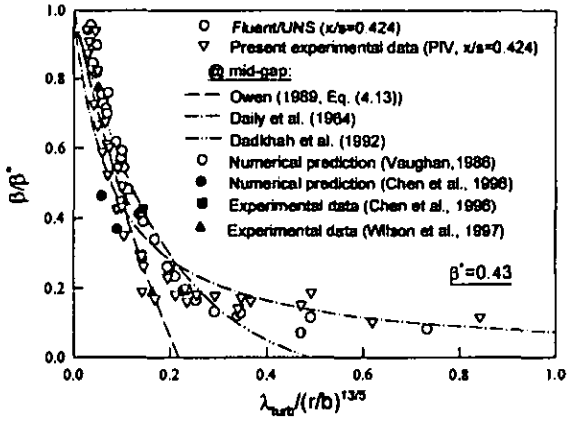

Fig. 8 Variation of β/β^* at or near mid-gap with $\lambda_{turb}/(r/b)^{13/5}$ ($0.4<r/b<t$, $1504\le c_w\le 7520$, $5.16\times10^5\le Re_\phi\le 9.55\times10^5$, $Re_m=5.0\times10^5$)

The measured and computed values of the fluid mean tangential velocity near the cavity mid-axial gap (x/s = 0.424) for the experiments of Table 1 are plotted in the nondimensional plane (β/β^*, $\lambda_{turb}/(r/b)^{13/5}$) suggested by Owen and Rogers (1989) in Fig. 8. The value $\beta^* = 0.43$ corresponds to the value of β at $\lambda_{turb} = 0$. Also shown in the figure are some of the measurements, correlations, and computational results reported by earlier researchers. Except for the range $0.1<\lambda_{turb}/(r/b)^{13/5}<0.3$, the empirical correlation of Daily et al. (1964) is seen to work quite well.

Static Pressure Distributions

The measured circumferential distributions of static pressure for Experiment 5 are shown in Fig. 9 : those at the radially outermost pressure tap location on the stator disk (r = 187.3 mm, r/b = 0.95), and at two axial positions on the outer shroud (5.1 mm and 13.4 mm downstream of the vane trailing edge plane). Pressure tap locations #1, 6, and 11 are identified in Fig. 2(b). The circumferential pressure asymmetry produced by the vanes and the decay of its strength axially downstream can be seen. At 5.1 mm downstream of the vane trailing edge plane, the peak pressure at the outer shroud (pressure taps 2 and 7) is in the wake region. There is no discernible circumferential pressure variation at the stator disk, indicating that the pressure asymmetry in the mainstream flow has been dissipated across the discouragers.

In Fig. 10(a), the measured and computed peak-to-peak amplitudes of the circumferential pressure asymmetry at the outer shroud are shown versus the distance downstream of the vane trailing edge plane for Experiments 6 and 7. The agreement between the measurements and the predictions is fair. The amplitude, of course, increases with the mainstream flow rate (a squared dependence).

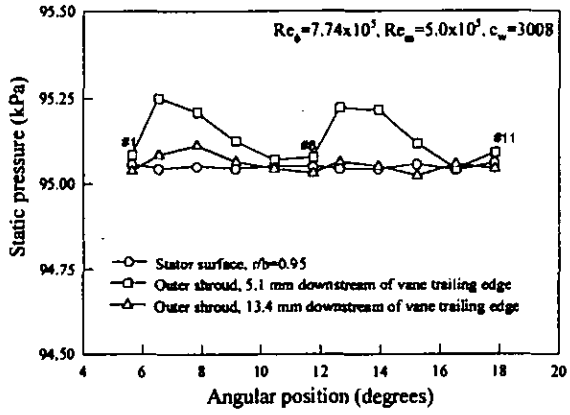

Fig. 9 Measured circumferential distribution of static pressure at the outer shroud and at the stator disk surface near the discourager (p_{atm}≈97.84 kPa)

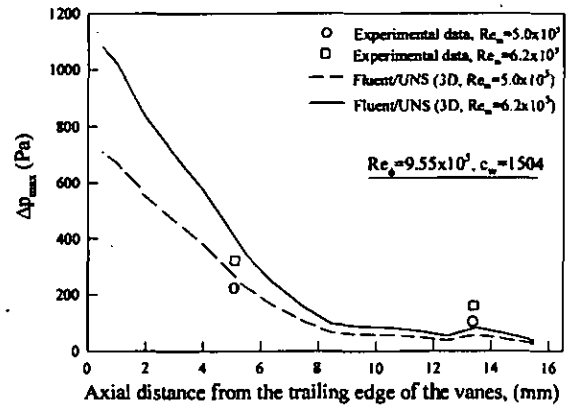

(a) Peak-to-peak amplitude, Δp_{max}

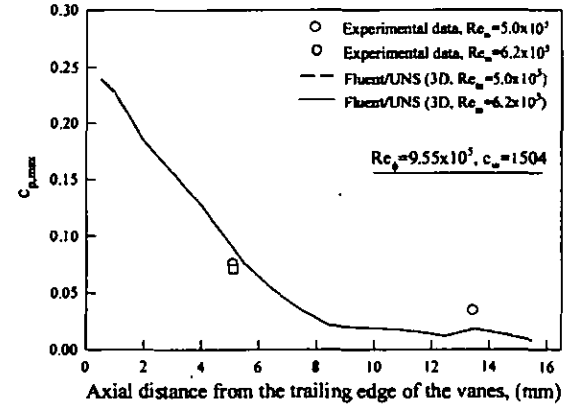

(b) Pressure coefficient, $c_{p,max}$

Fig. 10 Effect of main flow rate on the circumferential pressure asymmetry at the outer shroud

The pressure coefficient,

$$c_{p,min} = 2\,\Delta p_{min}/(\rho c_i^2) \qquad (2)$$

has a magnitude of approximately 0.25 at the vane exit, Fig. 10(b), diminishing to less than 0.01 at 16 mm downstream.

The effect of rotor disk speed on the radial distribution of static pressure in the cavity is shown in Fig. 11. Both the measured and computed values of pressure are at the stator disk surface. The secondary air flow rate is low (c_w = 1504), permitting a significant rotation of the core fluid. A qualitative understanding of the distribution can be obtained from a simplified version of the fluid radial momentum equation:

$$\partial p/\partial r \approx -\rho V_{r,c}(\partial V_{r,c}/\partial r) + \rho V_{\varphi,c}^{\ 2}/r \qquad (3)$$

At a particular secondary air flow rate, the core fluid tangential velocity increases with the rotor disk speed resulting in a larger $\partial p/\partial r$ magnitude. This characteristic can be seen in Fig. 11 in the radially outboard half of the cavity. A radial pressure profile such as for $Re_\phi = 9.55\times10^5$ can facilitate ingress of the mainstream gas into the cavity.

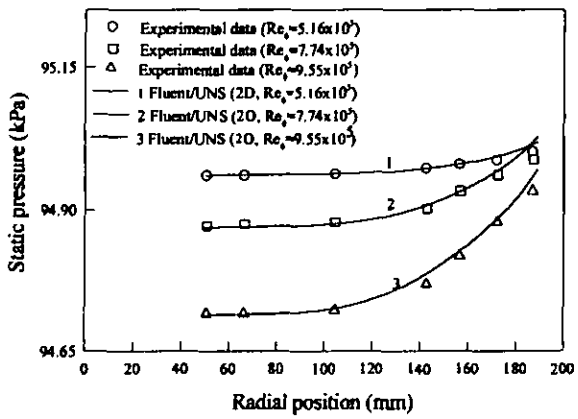

Fig. 11 Effect of Re_ϕ on the static pressure distribution at the stator disk surface for c_w=1504 and Re_m=5.0×10^5 (p_{atm}=97.84 kPa)

Figures 12(a) and (b) show, at two different rotor speeds, the influence of the secondary air flow rate on the disk cavity pressure distribution. The three pressure distributions in Fig. 12(a) correspond to the three tangential velocity profiles shown ia Fig. 6(a). The progressive suppression of core fluid rotation as the secondary air flow rate increases leads to the pressure distributions of Fig. 12(a). As c_w increases the absolute pressure level in the cavity rises. The same features can be observed in Fig. 12(b).

CONCLUSIONS

Particle image velocimetry was used to measure the fluid velocity field in a model rotor-stator disk cavity with a large axial gap ratio (G ≈ 0.08). The experiments ranged over 5.16×10^5 ≤ Re_ϕ ≤

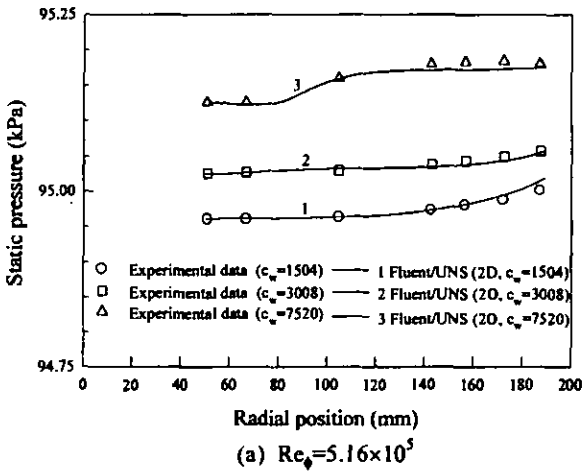

(a) Re_ϕ=5.16×10^5

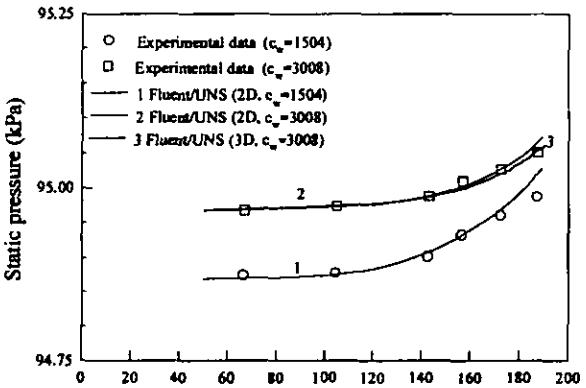

(b) Re_ϕ=7.74×10^5

Fig. 12 Effect of c_w on the static pressure distribution at the stator disk surface for Re_m=5.0×10^5 (p_{atm}=97.84 kPa)

9.55×10^5, 5.0×10^5 ≤ Re_m ≤ 6.2×10^5, and 1504 ≤ c_w ≤7520. Also measured were the static pressure distributions in the cavity at the stator disk and at the mainstream passage outer shroud. Two-dimensional (rotationally symmetric) as well as three-dimensional, with azimuthally periodic (following the vane pitch) boundary conditions, computations of the flow field were performed using the commercial CFD code FLUENT/UNS and compared with the measurements. Of the seven experiments discussed in this paper, all had secondary air flow rates smaller than the free disk pumping flow rate although in one case (Experiment 3) the secondary air flow rate was approximately 92 percent of the free-disk pumping flow rate.

The disk cavity axial gap was sufficiently large for separate boundary layers to form on the two disks. A recirculation region develnped radially inboard in the cavity where a strong radial outflow was found close to the rotor disk and a weak radial inflow near the stator disk. In this region, dubbed the source region, rotation of the core fluid was minimal. The radial extent of this region increased with the secondary air flow rate and decreased slightly as the rotor disk speed increased. Radially outboard, in the core region,

the flow was dominated by the tangential velocity except when the secondary air flow rate was high (close to the free disk pumping flow rate - for example, Experiment 3).

A circumferentially periodic pressure distributinn was found in the mainstream flow path, the periodicity following the vane pitch. The peak-to-peak amplitude of this asymmetry increased as the square of the main flow rate. The pressure coefficient, $c_{p,max}$, had a magnitude of approximately 0.25 at the vane exit and decayed rapidly downstream. Both the secondary air emerging from the disk cavity through the discourager radial clearance and the rotor blades affect this pressure coefficient decay.

In the experiments performed, no circumferential pressure asymmetry could be found in the disk cavity, even near its rim. The radial distribution of static pressure in the cavity depended strongly on the core fluid tangential velocity. The rotating fluid core gave rise to an adverse radial pressure gradient, its magnitude increasing as the rotation increased with decreasing secondary air flow rate. This feature facilitates ingress of mainstream gas into the cavity.

Two-dimensional (rotationally symmetric) simulation of the disk cavity and mainstream flow fields was carried out using the commercial CFD code FLUENT/UNS. A two-layer (near-wall, away-from-wall) description of the flow domain was used along with RNG k-ε model of turbulence. Three-dimensional calculations over one vane pitch were also performed using the same code, with a wall function replacing the near-wall description. Generally, good agreement was found between the measurements and the simulation results.

ACKNOWLEDGMENTS

This research was performed under subcontract no. 95-01-SR033 sponsored by the U.S. Department of Energy – Federal Energy Technology Center through a cooperative agreement with the South Carolina Institute for Energy Studies at Clemson University. A grant from AlliedSignal Engines, Phoenix, AZ during the initial phase of this work is also gratefully acknowledged.

REFERENCES

Bhavnani, S.H., Khodadadi, J.M., Goodling, J.S., and Waggott, J., 1992, "An Experimental Study of Fluid Flow in Disk Cavities," *ASME Journal of Turbomachinery*, Vol. 114, pp. 454-461.

Bohn, D., Johann, E., and Kruger, U., 1995, "Experimental and Numerical Investigations of Aerodynamic Aspects of Hot Gas Ingestion in Rotor-Stator Systems with Superimposed Cooling Mass Flow," ASME paper No. 95-GT-143, International Gas Turbine and Aeroengine Congress and Exposition, Houston, Texas.

Chen, J-X., Gan, X., and Owen, J.M., 1996, "Heat Transfer in an Air-Cooled Rotor-Stator System," *ASME Journal of Turbomachinery*, Vol. 118, pp. 444-451.

Chew, J.W., 1985, "Prediction of Flow in a Rotating Cavity With Radial Outflow Using Mixing Length Turbulence Model," Proceedings of the 4th International Conference on Numerical Methods in Laminar and Turbulent Flows, Swansea, Pineridge Press, pp. 318-329.

Chew, J.W. and Snell, R.J., 1988, "Prediction of the Pressure Distributioa for Radial-Inflow Between Co-Rotating Disks," ASME Paper No. 88-GT-127.

Chew, J. W., Green, T, and Turner, A. B., 1994, "Rim Sealing of Rotor-Stator Wheelspaces in the Presence of External Flow," ASME Paper No. 94-GT-126, International Gas Turbine and Aeroengine Congress and Exposition, The Hague, Netherlands.

Dadkhah, S., Turner, A.B., and Chew, J.W., 1992, "Perfnrmance of Radial Clearance Rim Seals in Upstream and Downstream Rotor-Stator Wheelspaces," *ASME Journal of Turbomachinery*, Vol. 114, pp. 439-445.

Daily, J.W. and Nece, R.E., 1960, "Chamber Dimension Effects on Induced Flow and Frictional Resistance of Enclosed Rotating Disk," *ASME Journal of Basic Engineering*, Vol. 82, pp. 217-232.

Daily, J.W., Ernst, W.D., and Asbedian, V.V., 1964, "Enclosed Rotating Discs With Superimposed Throughflow," Report No. 64, Department of Civil Engineering, Hydrodynamics Laboratories, Massachusetts Institute of Technology, Cambridge, MA.

Fluent Inc., 1998, "Computational Fluid Dynamics Software-FLUENT/UNS," *User's Guide, Release 4.2*, Lebanon, NH.

Gosman, A.D., Lockwood, F.C., and Loughhead, J.N., 1976, "Prediction of Recirculating, Swirling, Turbulent Flow in Rotating Disc Systems," *Journal of Mechanical Engineering Science*, Vol. 18, pp. 142-148.

Green, T. and Turner, A. B., 1994, "Ingestion into the Upstream Wheelspace of an Axial Turbine Stage," *ASME Journal of Turbomachinery*, Vol. 116, pp. 327-332.

Hill, N. J., Green, T., and Turner, A. B., 1997, "Aerodynamics of turbine rim seal ingestion," ASME paper No. 97-GT-268, International Gas Turbine and Aeroengine Congress and Exposition, Orlando, Florida.

Ho, Y.-H., Athavale, M.M., Forry, J.M., Hendricks, R.C., and Steinetz, B.M., 1996, "Numerical Simulatinn of Secondary Flow in Gas Turbine Disk Cavities, Including Conjugate Heat Transfer," ASME Paper No. 96-GT-67.

Ko, S.H. and Rhode, D.L., 1992, "Thermal Details in a Rotor-Stator Cavity at Engine Conditions With a Mainstream," *ASME Journal of Turbomachinery*, Vol. 114, pp. 446-453.

Louis, J.F. and Salhi, A., 1989, "Turbulent Flow Velocity Between Rotating Co-axial Disks of Finite Radius," *ASME Journal of Turbomachinery*, Vol. 111, pp. 333-340.

Owen, J.M. and Rogers, R.H., 1989, Flow and Heat Transfer in Rotating-Disc Systems. Vol. I: Rotor-Stator Systems, Research Studies Press, Taunton, United Kingdom.

Owen, J.M., 1989, "An Approximate Solution for the Flow Between a Rotating and a Stationary Disk," *ASME Journal of Turbomachinery*, Vol. 111, pp. 323-332.

Phadke, U. P. and Owen, J. M., 1988, "Aerodynamic Aspects of the Sealing of Gas-Turbine Rotor-Stator Systems, Part 3: The Effect of Nonaxisymmetric External Flow on Seal Performance," *International Journal of Heat and Fluid Flow*, Vol. 9(2), pp. 113-117.

Roy, R.P., Agarwal, V., Devasenathipathy, S., He, J., Kim, Y. W., and Howe, J., 1997, "A Study of the Flow Field and Convective Heat Transfer in a Model Rotor-Stator Cavity," *Experimental Methods in Heat Transfer*, HTD-Vol. 353, pp. 97-107, ASME Winter Annual Mtg., Dallas.

Vaughan, C., 1986, "A Numerical Investigation into the Effect of an External Flow Field on the Sealing of a Rotor-Stator Cavity," Ph.D thesis, University of Sussex.

Virr, G.P., Chew, J.W., and Coupland, J., 1993, "Application of Computational Fluid Dynamics to Turbine Disc Cavities," ASME Paper 93-GT-89, International Gas Turbine and Aeroengine Congress and Exposition, Cincinnati, Ohio.

Von Karman, T., 1921, "Uber Laminare und Turbulente Reibung," Z.Angew.Math.Mech., 1, p.233.

Wilson, M., Pilbrow, R., and Owen, J.M., 1997, "Flow and Heat Transfer in a Preswirl Rotor-Stator System." *ASME Journal of Turbomachinery*, Vol. 119, pp. 364-373.